Journal of Thermal Science Vol.30, No.4 (2021) 1376−1387

https://doi.org/10.1007/s11630-021-1488-2 **Article ID: 1003-2169(2021)04-1376-12**

Effects of Squealer Geometry of Turbine Blade Tip on the Tip-Leakage Flow and Loss

ZENG Fei[1], ZHANG Weihao[1*], WANG Yufan[1], CAO Xia[1], ZOU Zhengping[1,2]

1. National Key Laboratory of Science and Technology on Aero-Engine Aero-thermodynamics, School of Energy & Power Engineering, Beihang University, Beijing 100191, China
2. Research Institute of Aero-Engine, Beihang University, Beijing 100191, China

Abstract: The effective control of the tip-leakage flow and loss is of great significance to improve the aerodynamic performance of the turbine. In this paper, the evolution mechanism of tip-leakage flow in a transonic high pressure turbine with a squealer tip is investigated with numerical simulation methods. The impacts of squealer geometric, such as the inclined pressure side rim and squealer rim width, on the vortex structure in the gap and tip-leakage loss are discussed. The results show that the scraping vortex inside the cavity plays the role of aero-labyrinth seal, and forms interlocking sealing labyrinth structure with the rims on both sides, which has an effective sealing effect on the tip-leakage flow. The inclined pressure side squealer rim inhibits the development of the pressure side squealer corner vortex, which is beneficial to expand the influence range of the scraping vortex and enhance the sealing effect on the tip-leakage flow. The increase of the suction side squealer rim width reduces the effective flow area at the gap exit, which is conducive to reduction of the tip-leakage flow rate and tip-leakage loss. However, the increase of the pressure side squealer rim width strengthens the pressure side squealer corner vortex and limits the development space of the scraping vortex, causing the adverse effects on the control of tip-leakage flow.

Keywords: turbine, squealer tip, tip-leakage flow, squealer width, tip-leakage loss

1. Introduction

The tip-leakage flow of the rotor blade tip has adverse effects on the turbine in many ways, which are mainly reflected in five aspects: (1) the load on the rotor blade tip is reduced; (2) the flow loss of the rotor passage is increased; (3) the effective flow area of the rotor passage is reduced; (4) the inlet distortion of the downstream blade row is enhanced; (5) the thermal performance of the blade tip is deteriorated. Among these five major effects, the effect on the aerodynamic performance is particularly prominent, and related research [1] has shown that the loss raised by the tip-leakage flow can account for more than 30% of the total aerodynamic loss in the rotor passage. Therefore, the effective control of tip-leakage flow and tip-leakage loss is of great significance for improving aerodynamic performance of the turbine.

The optimization design of blade tip airfoil [2, 3] and different tip shape designs, such as squealer tip and winglet tip [4–6], are one of the commonly used control methods for tip-leakage flow. Common squealer tips

Received: Feb 22, 2020 AE: KAN Xiaoxu Corresponding author: ZHANG Weihao E-mail: zhangweihao@buaa.edu.cn

Nomenclature

C	chord/m	ρ	density/kg·m^{-3}
H	cavity height/m	τ	gap height/m
Ma	Mach number	**Subscript**	
$\dot{m}$	mass flow rate/kg·s^{-1}	2,exit	rotor outlet
N	airfoil count	inlet	stator inlet
P	pressure/Pa	inner	inner of gap
Re	Reynolds number ($(\rho V)_{\text{exit}} C\mu^{-1}$)	leakage	tip-leakage flow
$\dot{S}'''_{g,\text{local}}$	local entropy production rate/W·m^{-3}·K^{-1}	n	normal to camber
s	entropy/J·K^{-1}·kg^{-1}	notip	condition without tip
T	temperature/K	outer	outer of gap
t	squealer width/m	p	pressure side squealer
V	velocity/m·s^{-1}	passage	rotor passage
Y	leakage loss/J	r	relative
Greek symbols		s	suction side squealer
η	efficiency	t	tangential to camber
μ	dynamic viscosity/N·s·m^{-2}	tip	condition with tip
ξ	normalized leakage loss	**Superscript**	
π	total-to-total pressure ratio	*	stagnation parameter

have three typical geometries, tips with a pressure side squealer, a suction side squealer and a double side squealer. The double side squealer tip, which is referred as "squealer tip" in this paper, has been proved to have excellent aerodynamic and heat transfer performance with the deepening of the research [7–12]. Earlier, Dey et al. [13] studied the single-squealer tips and found that the suction side squealer tips have a better blocking effect on tip-leakage flow. Sumanta et al. [14] studied a variety of single-squealer tips and double-squealers tips and found that the suction side squealer tips have the best aerothermal performance. However, researches by Krishnababu et al. [15] shown that, the double side squealer tips can play a better role in reducing the tip-leakage flow rate, because of the double-blocking effect on tip-leakage flow raised by the double side squealer. Zhou [16] found that the tip-leakage loss coefficient of the double side squealer tip was significantly lower than that of the flat tip through numerical simulation methods and plane cascade experiments, which proved that the double-blocking effect in the double side squealer tip is beneficial for reducing tip-leakage loss.

In the further study of the squealer tip, the flow mechanism of the squealer tip became the focus. Yang [17, 18], and Virdi et al. [19] found that the relative movement of the casing could account for a new vortex structure in the cavity. Mischo et al. [20] optimized the cavity geometry and improved the aero-thermal performance of the squealer tip through a detailed analysis of the flow field inside the cavity. And the research showed that there are three dominant flow characteristics in the cavity, which are scraping vortex (SV), the pressure side squealer corner vortex (PSCV) and the suction side squealer corner vortex (SSCV). Zhou [21] further confirmed this by studying the evolution of the flow field in the gap of the squealer tip. Shao [22] combined the theoretical analysis with numerical simulation to analyze the effects of many vortices inside the cavity on the tip-leakage flow, and proposed that the scraping vortex is the dominant flow structure that plays a critical role in blocking the tip-leakage flow. The Von Karman Institute for Fluid Dynamics (VKI) [23] performed a vortex identification study on its unique multi-cavity squealer-like tip, confirming the control effect of the complex vortex structure inside the cavity on the tip-leakage flow.

In the research on the geometric optimization of squealer tips, Gao et al. [24] added rims with different directions in the squealer tip, and found that adding transverse rims into the cavity could enhance the separation of airflow and raise new vortex inside the cavity, increasing the blocking effect on the tip-leakage flow. Nikolay et al. [25, 26] studied the effects of squealer tip with rim cut-off at different positions on the tip-leakage flow. Studies have shown that the squealer tips with suction side squealer rim cut-off have higher stage efficiency. Zhou [27] and Senel et al. [28] studied the aero-thermal effects of the squealer width and height on the tip-leakage flow with numerical methods. Prakash

et al. [29] found that the squealer tip with inclined pressure side squealer rim could control the tip-leakage flow by increasing the blocking area at the gap inlet. Researchers at VKI [30–32] optimized the squealer-like tip with differential evolution optimization strategy and obtained the shape of the multi-cavity squealer-like tip with excellent aerodynamic performance. From the results of these studies, it is clear that the geometric optimization of squealer tips has achieved great results. However, the inter-relationship among squealer geometry, vortex structure, aerodynamic parameters of tip-leakage flow, and tip-leakage loss needs to be explored thoroughly in order to confirm the influence mechanism of squealer geometry on tip-leakage flow.

In this paper, a single-stage transonic high pressure turbine with squealer tip is considered as the research object. The control mechanism of the squealer tip on tip-leakage flow is summarized by comparing the difference of flow structure in the gap and aerodynamic performance between turbine with flat tip and turbine with squealer tip. Further, the effects of squealer geometry, such as the inclination of the pressure side squealer rim and squealer width, on the tip-leakage loss and the aerodynamic performance are studied with the analysis of the vortex structure in the gap, the tip-leakage flow rate and momentum at the gap exit.

2. Numerical Details

2.1 Turbine in study

The turbine geometry in this study is a transonic single stage high-pressure turbine. The main geometric parameters and the operation conditions of the turbine stage are listed in Table 1.

Table 1 Turbine parameters and boundary conditions

	N	Aspect ratio	τ/%span
Stator	46	0.6	–
Rotor	72	1.15	1.16%
Blade passing frequency/HZ	π	$Ma_{r,exit}$	Re_{exit}
17 610	4.08	1.11	1.12×10^6

In order to study the influence of squealer geometry on tip-leakage flow, the flat tip (Case 1) of the turbine rotor blade is modified. Five kinds of squealer geometry with different squealer rim inclination and squealer width are obtained. With the exception of Case 1 and Case 2, the blade tip geometry in the other cases all have inclined pressure squealer. The geometric parameters are shown in Fig. 1. Cavity depth (H) of all the squealer tip cases is 1.5τ. The geometric characteristics of Cases 2–6 are shown in Table 2.

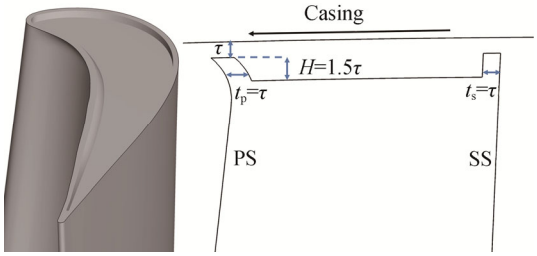

Fig. 1 Sketch of blade tip geometry with inclined pressure side squealer

Table 2 The geometric characteristics of Cases 2–6

Case number	Case 2	Case 3	Case 4	Case 5	Case 6
Pressure side squealer rim width (t_p)	τ	τ	7.2τ	4.1τ	τ
Suction side squealer rim width (t_s)	τ	τ	τ	4.1τ	7.2τ
Pressure side squealer inclined or not	No	Yes	Yes	Yes	Yes

2.2 Computational approach

The numerical simulation in this study uses the software ANSYS CFX 12.0 to solve steady viscous Reynolds Averaged Navier-Stokes equations with the Shear Stress Transport (SST) turbulence model to close equations. The solver uses the time pursuing finite volume method, and the spatial discretization uses a second order upwind scheme. The computational domain consists of one stator channel and one rotor channel. Total temperature, total pressure and turbulence intensity are used as the inlet boundary conditions, and inflow direction is normal to boundary condition. As the outlet boundary condition, static pressure can be adjusted to make sure certain total-to-total pressure ratio. Both surfaces at the circumferential side of the stator and the rotor channels are set as periodic boundary conditions. And surface between stator and rotor is set as mixing-plane. All the wall faces are set as adiabatic with no slip. The numerical method has been validated in Ref. [33].

2.3 Grid independence validation

The commercial software NUMECA Autogrid 5 is used to generate the stator domain computational grid, and the ICEM is used to generate the rotor domain computational grids. The mesh elements in both domains are hexahedrons. Local encryption is carried out near the shroud, the hub and the rotor blade. The wall distance of first mesh cell is set to 0.001 mm, and the average value of calculated y^+ is about 3. To eliminate the influence of different grid topology on the numerical results, all the cases use the same stator domain computational grid and

the same topological structure is used in the rotor domains of all the cases. The grids are shown in Fig. 2.

Considering that the grid density may affect the accuracy of the numerical results, grid independence validation is performed. A total of 11 grids are verified, among which the Grid 1–5 are used to verify the grid independence of main flow and the Grid 6–11 are used to verify the grid independence of gap flow.

The grid number and the simulated turbine stage efficiency of Grid 1–5 are shown in Table 3. Fig. 3 shows the effect of grid number in main flow region on turbine stage efficiency. When the number of grids reaches 2.72 million, the turbine stage efficiency no longer changes significantly with the increase of grid number. Considering the accuracy of simulation and the effective use of computing resources, the grid with 2.72 million (Grid 3) is selected.

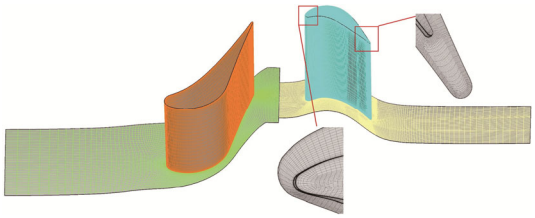

Fig. 2 Sketch of computational grid

Table 3 Total numbers and simulation results of varied grid

	Grid 1	Grid 2	Grid 3
Total number/10^6	2.04	2.36	2.72
Turbine stage efficiency	87.27%	87.25%	87.23%
	Grid 4	Grid 5	
Total number/10^6	3.05	3.37	
Turbine stage efficiency	87.24%	87.23%	

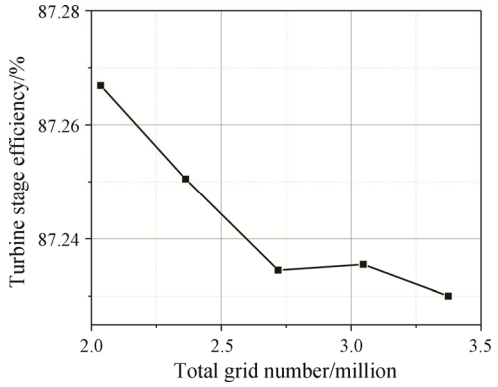

Fig. 3 Influence of total grid number on turbine stage efficiency

In addition, because the research object is mainly tip-leakage flow, the radial grid number in the rotor tip is analyzed and determined. The six cases of different gap grid density are calculated in the turbine with flat tip. The grid distribution of each case is shown in Table 4.

A comparison of tip-leakage flow rate of Grid 6–11 is shown in Fig. 4. As the data show, with the increase of grid number, the difference of tip-leakage flow rate between two adjacent cases decreases gradually. When the number of radial grids in the gap is more than 31, the differences of tip-leakage flow rate are less than 0.06%, which can be ignored. Therefore, it can ensure the accuracy of the numerical results and save the computation cost as much as possible to determine the radial grid number in the gap as 31.

Table 4 Cases of varied mesh allocation

	Axial×Tangential×Radial		Total Number /10^6
	stator	Rotor (gap)	
Grid 6	156×40×56	214×43×90 (13)	2.39
Grid 7		214×43×96 (19)	2.57
Grid 8		214×43×102 (25)	2.74
Grid 9		214×43×108 (31)	2.92
Grid 10		214×43×114 (37)	3.10
Grid 11		214×43×120 (43)	3.28

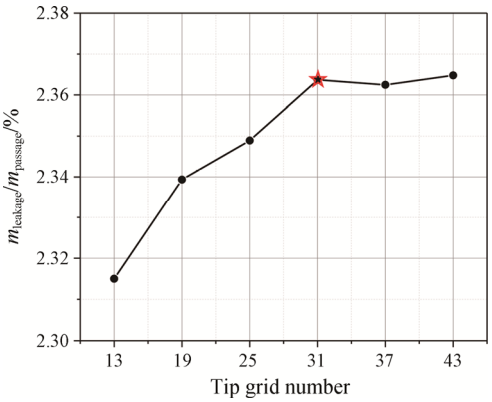

Fig. 4 Influence of local grid density of blade tip on tip-leakage flow rate

3. Results and Discussion

3.1 Evaluation and comparison of aerodynamic performance

In this study, the tip-leakage loss is estimated by the difference between the entropy increase in the rotor passage under the gap condition and the gapless condition. Tip-leakage loss is composed of the mixing loss outside the gap and the internal loss of the gap measured by the entropy increase at the inlet and exit of the gap. The loss of each part can be expressed as:

$$Y_{tip} = \dot{m}_{passage} T_2 \Delta s - \dot{m}_{passage\_notip} T_{2\_notip} \Delta s_{notip} \quad (1)$$

$$Y_{tip\_inner} = \dot{m}_{leakage} T_{tip} \Delta s_{tip} \quad (2)$$

$$Y_{\text{tip\_outer}} = Y_{\text{tip}} - Y_{\text{tip\_inner}} \quad (3)$$

The dimensionless loss coefficient ξ, which is used for comparison, is defined as the ratio of the loss to the total loss of the rotor passage without gap. The aerodynamic performance parameters of each case are shown in Table 5.

Table 5 Comparison of aerodynamic performance parameter

Number	ξ	$\frac{\dot{m}_{\text{leakage}}}{\dot{m}_{\text{passage}}}$	$\xi_{\text{tip\_inner}}$	$\xi_{\text{tip\_outer}}$	ξ_{tip}
Case 1	87.23%	2.36%	3.20%	26.30%	29.5%
Case 2	87.49%	2.03%	3.76%	21.26%	25.0%
Case 3	87.57%	1.92%	3.90%	19.96%	23.9%
Case 4	87.59%	2.05%	4.02%	19.79%	23.8%
Case 5	87.56%	2.09%	3.75%	20.75%	24.5%
Case 6	87.67%	1.93%	4.15%	18.61%	22.8%

The difference in turbine stage efficiency of each case in Table 5 shows that the squealer tip can improve the turbine stage efficiency by 0.26% compared to the flat tip. However, the turbine stage efficiency increase caused by the geometric optimization based on the conventional squealer tip is smaller. Both the inclined pressure side squealer rim and the widened suction side squealer rim can increase the turbine stage efficiency by about 0.1%. According to the loss components of Case 1, Case 2, Case 3, and Case 6, it can be found that as the turbine stage efficiency increases, the internal loss of the gap gradually increases, while the external loss of the gap decreases, and the total tip-leakage loss shows a downward trend. It can be seen that the squealer tip reduces the mixing loss between tip-leakage flow and the mainstream by increasing the mixing inside the gap.

3.2 Influence of inclined pressure side squealer rim on tip-leakage flow

Omega method is very helpful to capture both strong and weak vortices and analyze the vortex structures in turbine rotor passage comprehensively [34]. Fig. 5 shows the vortex structures of Cases 1–3 inside the cavity identified by the Omega method [35], and the vortex structures are colored with the streamwise vorticity (the component of vorticity along the flow direction). The evolution of vortex structures, such as SV and PSCV, of the squealer tips (Case 2 and Case 3) are similar. However, there is only a less obvious scraping vortex structure in the flat tip. Compared with Case 2, the size of the SV in Case 3 is larger, and this phenomenon is especially obvious near the trailing. In addition, the PSCV in Case 3 has been significantly suppressed, which is conducive to obtaining greater development space for the SV.

Based on the previous work of our research team [22], the flow structures of squealer tip inside the cavity can be summarized into four typical two-dimensional flow topologic structures, as shown in Fig. 6(b). The effective control of the squealer tip on the tip-leakage flow mainly depends on the B & C-type flow topologic structures. The blocking effect of C-type flow structure on tip-leakage flow is particularly prominent. In the range of C-type flow structure, the SSCV gradually disappears, and the range of the PSCV gradually expands. The SV, which plays the role of aero-labyrinth seal, moves to the suction side squealer rim (SSSR), resulting in the effect similar to reduction of the gap between the teeth of the labyrinth sealed structure, thereby better blocking the tip-leakage flow.

The velocity vectors and Mach number distributions at the sections of 83% and 90% streamwise position in the Case 2 and Case 3 are shown in Fig. 7. At the 83% streamwise position, the PSCV of the conventional squealer tip occupies most of the space inside the cavity, which caused the size of the SV to be suppressed and forced the SV to move to the SSSR. Therefore, the flow topologic structure tends to be C-type. Different from Case 2, the PSCV of Case 3 is smaller, and the SV is located in the middle of the cavity, and the flow topologic

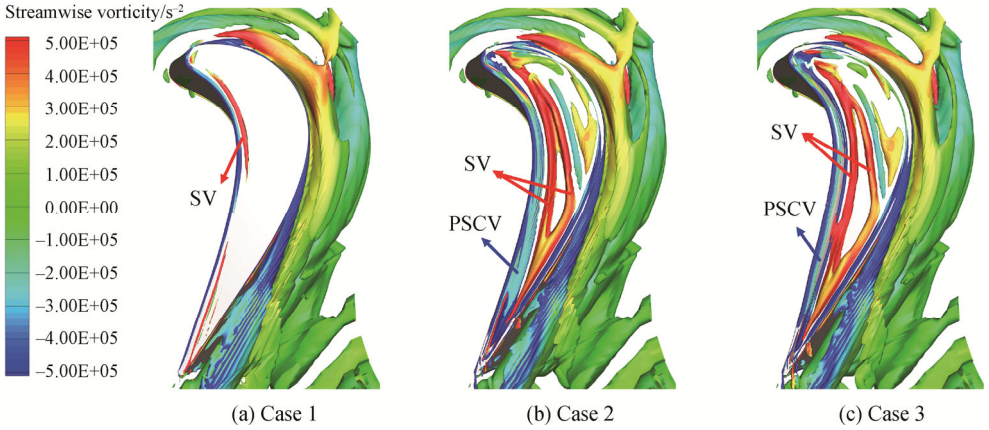

Fig. 5 Comparison of vortex structures in the gap

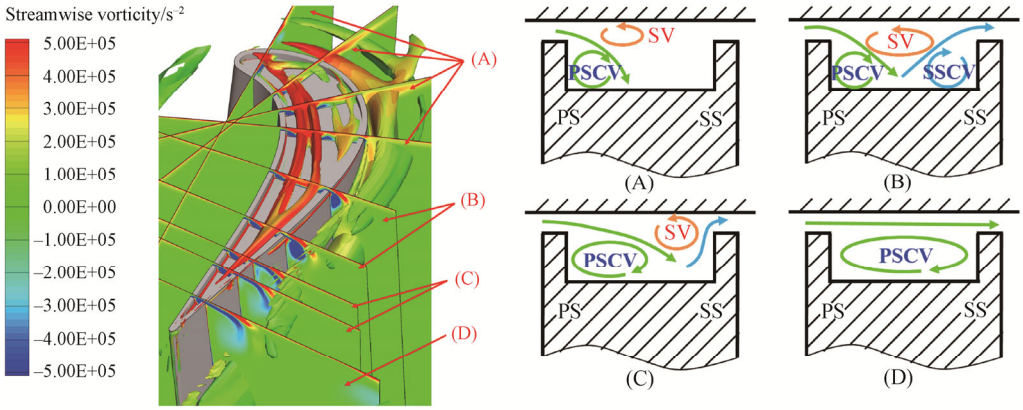

(a) SV inside the cavity (b) Typical flow topologic structures inside the cavity

Fig. 6 Vortex structures and topologic structures inside the cavity

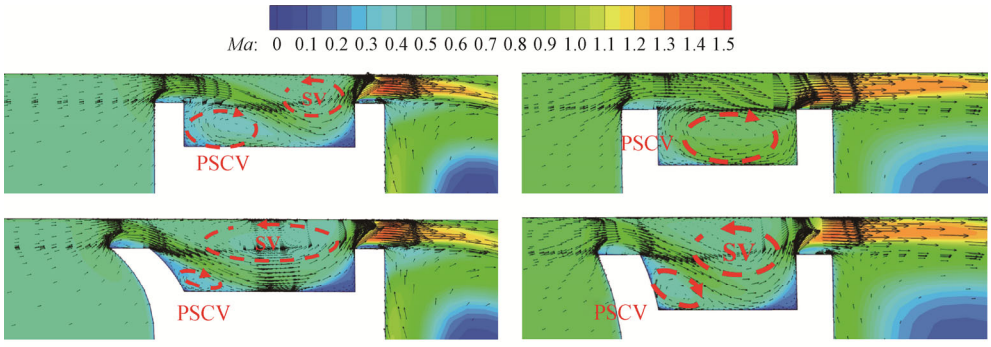

(a) 83% streamwise position (b) 90% streamwise position

Fig. 7 Mach number and velocity vector distribution ((a) Case 2; (b) Case 3)

structure tends to be B-type. As the vortex structures develop downstream, the SV of the conventional squealer tip has disappeared at 90% streamwise position, and the flow topologic structure is D-type, which means that the blocking effect of the vortex structure inside the cavity on the tip-leakage flow is weakened sharply. However, the SV in Case 3 is right next to the SSSR, and the flow topologic structure is C-type. It is clear that the evolutionary difference of the SV in Case 2 and Case 3 is affected by the evolution of PSCV.

Another significant flow characteristic in Case 3 is that the separation bubble at the top of the pressure side squealer rim (PSSR) becomes larger. At the two sections of different streamwise positions shown in Fig. 7, the incident of the airflow at the gap inlet in Case 3 is significantly larger than that in Case 2, and a larger separation bubble is formed, which causes the tip-leakage flow to flow into the cavity at a larger incident, and the PSCV is weakened accordingly. Therefore, the inclined pressure side squealer rim enhances the blocking effect on the tip-leakage flow by increasing the incident of the tip-leakage flow at the inlet of the gap, suppressing the PSCV, and expanding the development space of the SV.

The blocking effect of the vortex structure in the gap on the tip-leakage flow will be reflected in the distribution of the aerodynamic parameters of the tip-leakage flow at the gap exit, and finally affects the mixing loss caused by tip-leakage flow and main flow. According to the previous work of our research team [22], the mixing loss between tip-leakage flow and main flow can be estimated by:

$$T\Delta s = \frac{\dot{m}_{\text{leakage}}}{\dot{m}_{\text{passage}}}\left[\left(V_{\text{n}}-0\right)^2+\left(V_{\text{t}}-V_{\text{passage}}\right)^2\right] \quad (4)$$

The influence of the leakage flow rate and the velocity on mixing loss are comprehensively represented by momentum. Therefore, Fig. 8 shows the tip-leakage flow rate and momentum distributions along the streamwise direction at the gap exit. There are clear valleys in the tip-leakage flow rate and momentum distributions of the squealer tip at the 85%–95% streamwise position, and the location of the valley in Case 3 is slightly downstream than that of Case 2. The valley is caused by the sharp decrease in the blocking effect of the vortex structures inside the cavity on the tip-leakage flow due to the SV flowing out of the gap. The backward shift of the valley means that the position of the outflow gap of the SV in Case 3 moves slightly downstream, and the range of the SV exerting its blocking effect is relatively large.

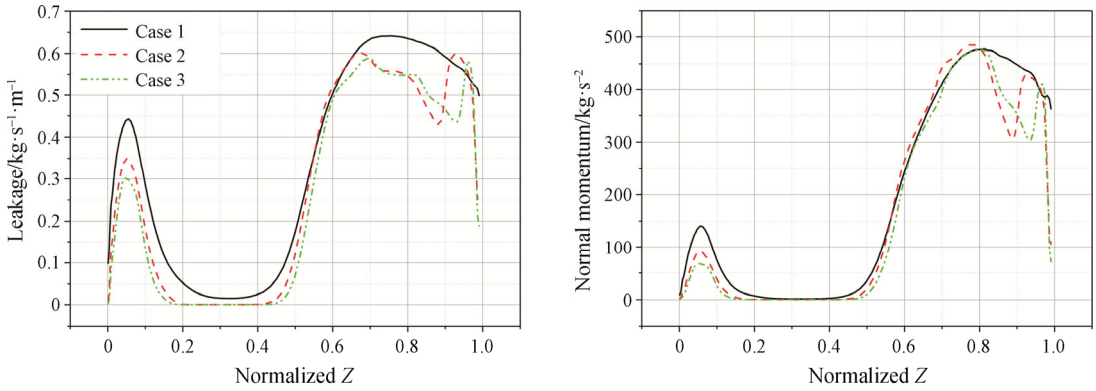

(a) Leakage flow rate per unit area (b) Normal momentum of tip-leakage flow

Fig. 8 Comparison of aerodynamic parameters distribution at the gap exit along the streamwise direction

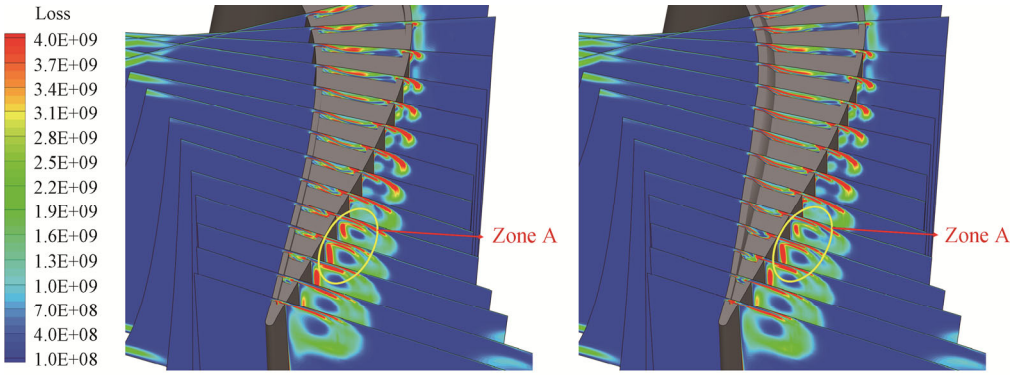

(a) Case 2 (b) Case 3

Fig. 9 Distribution of local entropy production in Case 2 and Case 3

The local loss can be measured by the local entropy production which can be expressed as [36]:

$$\dot{S}'''_{g,\text{local}} = \frac{\lambda}{T^2}\frac{\partial \overline{T}}{\partial x_i}\frac{\partial \overline{T}}{\partial x_i} + \frac{\alpha_t}{\alpha}\frac{\lambda}{\overline{T}^2}\frac{\partial \overline{T}}{\partial x_i}\frac{\partial \overline{T}}{\partial x_i} + \frac{2\mu \overline{s}_{ij}\overline{s}_{ij}}{\overline{T}} + \beta\frac{\rho\omega k}{\overline{T}} \tag{5}$$

where λ is the thermal conductivity; α_t and α represent the turbulent thermal diffusivity and the thermal diffusivity respectively; ω is the turbulent eddy frequency; k is the turbulent energy, and β=0.09.

The local entropy production distributions for Case 2 and Case 3 are shown in Fig. 9. The local entropy production caused by the mixing between tip-leakage flow and the mainstream in Case 2 and Case 3 are significantly different in zone A, which corresponds to the position of the difference in the aerodynamic parameters of the tip-leakage flow at the gap exit. It can be seen that Case 3 can effectively reduce the tip-leakage loss by strengthening the blocking effect on the leakage flow.

3.3 Influence of squealer width on tip-leakage flow

As shown in Table 5, compared with Case 3, the aerodynamic performance of the turbine stage in Case 4 and Case 5 have no significant change, while the turbine isentropic efficiency of Case 6 has improved by 0.1%. After the SSSR are widened, the internal gap loss coefficient is increased by 0.25% compared to Case 3, while the external mixing loss is reduced by 1.35%.

Fig. 10 shows the evolution of the SV inside the gap in four cases with different squealer width. Changes in the squealer width lead to corresponding changes in the cavity width, and the evolution of the vortex structures inside the cavity is more obviously limited by the circumferential space. In Fig. 10(a), the SV bifurcates and merges in the middle and rear sections of the cavity. From the distribution of the streamwise vorticity, the strength of the branch near the SSSR of the SV is relatively small, and its entrainment effect on the tip-leakage flow is weaker. With the increase of the squealer rim width, the bifurcation of the SV becomes less obvious, and the SV is closer to the SSSR. It can be seen from Fig. 10(b)–(c) that with the increase of the PSSR width, the separation bubble at the top of the PSSR increases. In addition, the SV is far from the PSSR, and the position of the SV outflow the gap is shifted upstream, and the ranges of the B&C-type flow topologic structures that can effectively block the tip-leakage flow are limited. Different from Case 4 and Case 5, as the SSSR widen, the distance between the SV and the PSSR in Case 6 has no significant

change. Therefore, although the cavity width is reduced, the SV still has sufficient circumferential development space near the trailing edge of the cavity, which also ensures that the SV has a larger range in the streamwise direction. In addition, the SV in Case 6 is stronger, to a certain extent, which is conducive to enhancing the entrainment effect of the SV on the tip-leakage flow, and the leakage flow can be blocked better.

Fig. 11 shows the tip-leakage flow rate and momentum distributions along streamwise direction with varied squealer width conditions. There are valleys in the tip-leakage flow rate and momentum distributions of Case 3 and Case 6 near the 90% streamwise position, while the valley of Case 5 is located near the 83% streamwise position. In order to analyze the cause of the valleys formation in depth, Fig. 12 shows the tangential velocity vector and Mach number distributions at the 83% and 90% streamwise positions. The Omega contours without band, which are conducive to analyzing the evolution of the vortex structures such as the SV, the PSCV and the SSCV, are also given in Fig. 12.

It can be seen from Fig. 11(a) that at the 83% streamwise position, the tip-leakage flow rate of Case 5 drops sharply, and then rises sharply at a slightly downstream position. In conjunction with Fig. 12(a), it can be found that there is no cavity in Case 5 at the 83% streamwise position, but there is a low Mach number area near the gap exit. This is because the cavity in Case 5 ends near the 83% streamwise position and the low-energy fluid with low velocity in the cavity flows out from the suction side close to the top of the blade. At the slightly downstream position, the tip-leakage flow is mainly the flow from the pressure side to the suction side with large speed, and the tip-leakage flow rate rises rapidly. At the 83% streamwise position, there are also obvious SV in the cavities of the other three cases. The SV in Case 4 is about to flow out of the gap, and the PSCV occupies most of the space inside the cavity. Comparing with Case 3, it can be found that the flow separation at the top of the PSSR in Case 4 is changed from open separation to closed separation. The incident of the tip-leakage flow into the cavity is small, and it is easy to form a larger size PSCV. The size of the SV in Case 6 is larger in the circumferential and radial directions, which has a stronger entrainment and blocking effect on the tip-leakage flow compared with Case 3.

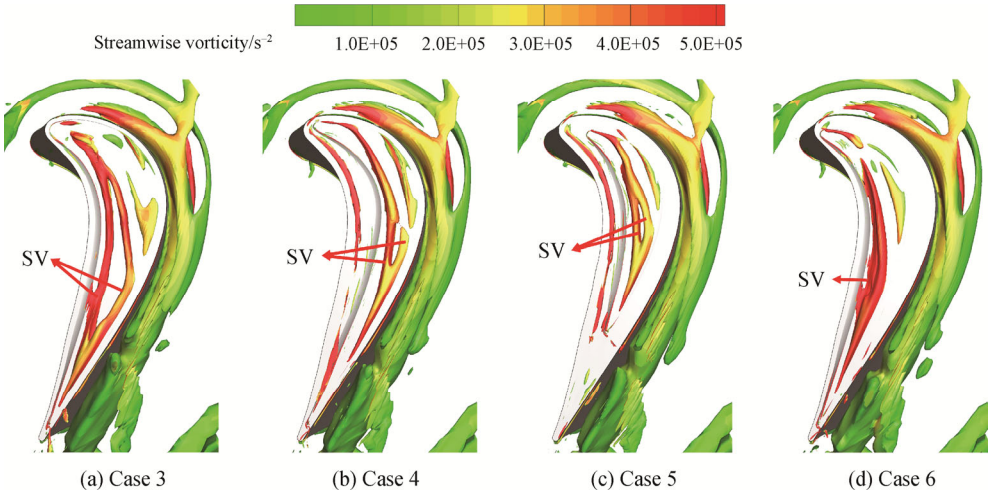

Fig. 10 Comparison of SV in cases with different squealer width

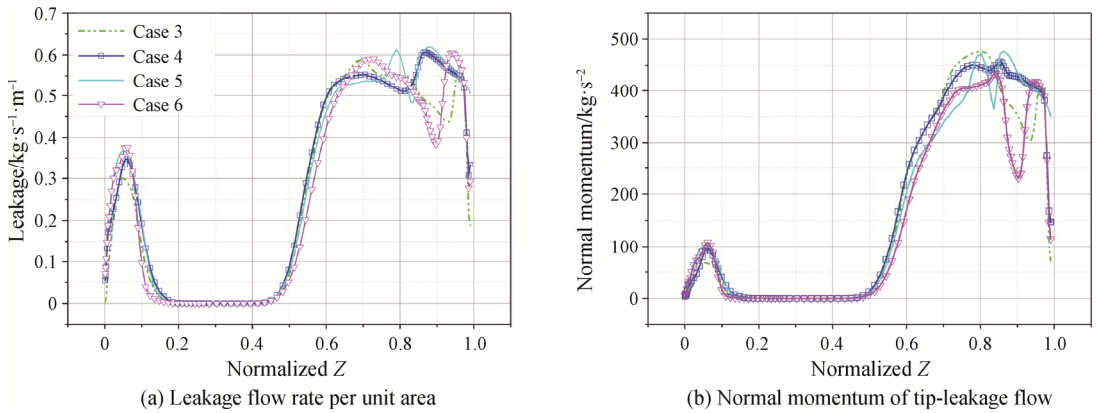

Fig. 11 Distributions of parameters at the gap exit along the streamwise direction

The Omega contours without band at the 90% streamwise position indicate that there is no longer a SV in the gap of Case 5, and the blocking effect on the tip-leakage flow has dropped sharply. With reference to Fig. 10(a) and Fig. 12(b), it can be known that the SV inside the cavity still maintains large and strong in Case 3 benefitting from the large cavity width. Therefore, at this streamwise position, Case 3 can still maintain good sealing performance and effective block effect on the tip-leakage flow. There is a small-sized SV with high intensity inside the cavity of Case 6. The SV and the double side squealer rims make up an interlocking labyrinth sealing structure, which is conducive to the formation of the open separation at the top of the SSSR, and the reduction of the effective flow area at the gap exit, and thus reduce the tip-leakage flow rate.

The entropy increase characterizes the local losses and losses transported from upstream to local and can be expressed as:

$$\Delta s = C_p \ln \frac{T}{T_{\text{ref}}} - R \ln \frac{p}{p_{\text{ref}}} \tag{6}$$

where C_p is the specific heat capacity at constant pressure, and the mass-weighted average pressure and temperature at the rotor inlet are taken for reference pressure p_{ref} and reference temperature T_{ref}, respectively.

Fig. 13 shows the distribution of limiting streamlines and the entropy increase caused by tip leakage vortex. At the 80% of axial chord, there is no significant difference among the entropy increase distributions of four cases, which indicates that the difference in the tip-leakage flow aerodynamic parameters upstream of the 80% of axial chord has not significantly affected the loss. At the 90%

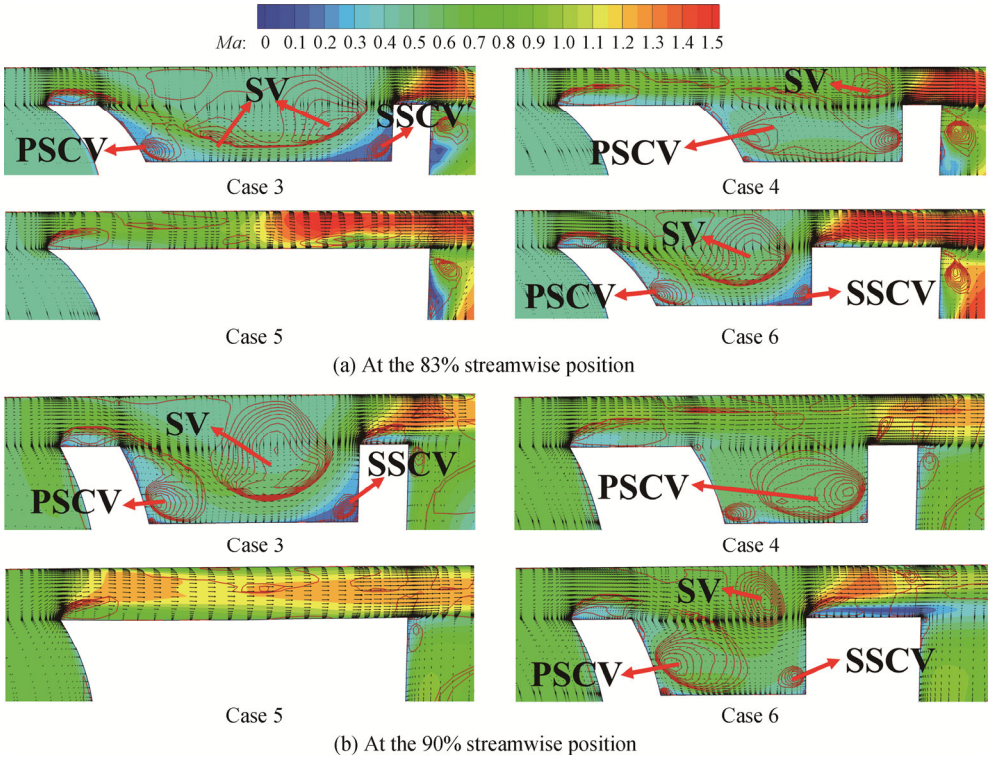

Fig. 12 Comparison of Mach number and velocity vector distribution (the contours without band: vortex structures identified by Omega method)

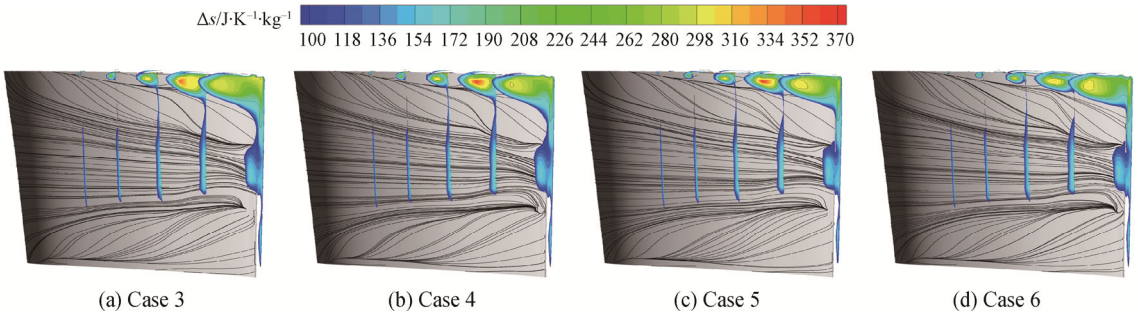

Fig. 13 Comparison of skin friction lines and entropy increase distribution

of axial chord, the entropy increase of Case 6 is significantly smaller than that of other examples, while the entropy increase of Case 4 and Case 5 is slightly higher than that of Case 3. According to the parameters distributions of the tip-leakage flow of each case in Fig. 11, it is clear that the reduction of the tip-leakage flow rate and momentum near the trailing edge can effectively reduce the entropy increase caused by tip leakage vortex.

In summary, the increase of the PSSR width will decrease the incidence angle of the tip-leakage flow when it enters the cavity, enhancing the PSCV, and suppressing the development space of the SV, which is not conducive to blocking the tip-leakage flow. The increase of the SSSR width will not have a significant effect on the PSCV, but will push the SV closer to the SSSR, which can expand the range of the C-type flow structure, suppress the tip-leakage flow and reduce the tip-leakage loss.

4. Conclusion

In this paper, a single-stage transonic high pressure turbine with squealer tip is taken as the research object. The influence of squealer geometry parameters, such as the inclined pressure side rim and squealer rim width, on tip-leakage flow is studied. Based on the analysis of the vortex structure evolution in the gap, the distribution of aerodynamic parameter at the gap exit and the aerodynamic performance parameter of the turbine, the influence mechanism of these geometric parameters on the tip-leakage flow are summarized. The main conclusions are as follows:

(1) The C-type flow structure and the open separation at the top of the suction side squealer rim are the key structure to reduce tip-leakage flow rate and momentum. The scraping vortex plays the role of aero-labyrinth seal, and forms interlocking sealing labyrinth structure with the rims on both sides. The scraping vortex is close to the suction side squealer rim, which leads to the formation of the C-type flow structure. Similarly, the gap between the teeth of the labyrinth sealed structure is reduced and the sealing effect is stronger. The open separation phenomenon at the top of the suction side squealer rim is also formed under the influence of the C-type flow structure, which can reduce the effective flow area at the gap exit and thus control the tip-leakage flow rate.

(2) The inclined pressure side squealer rim can effectively increase the size of the scraping vortex by suppressing the pressure side squealer corner vortex, thereby increasing its blocking effect on the tip-leakage flow. The inclined pressure side squealer rim increases the incident of the tip-leakage flow at the gap inlet, and the pressure side squealer corner vortex is suppressed. Development space of the scraping vortex is expanded, and the position of the scraping vortex out of the gap is moved to downstream, which expand the control range of the C-type flow structure, thereby effectively enhancing to its blocking effect.

(3) The increase of the suction side squealer rim width can effectively reduce the tip-leakage loss, while the increase of the pressure side squealer rim width has no obvious influence on the aerodynamic performance of the turbine. The suction side squealer rim enhances the blocking effect of the flow structure C on the tip-leakage flow by reducing the cavity width. The increase of the pressure side squealer rim width makes the open separation evolve into a closed separation at the top of the rim, increasing the size of the pressure side squealer corner vortex, reducing the circumferential and radial dimensions of the scraping vortex, and reducing the control range of the scraping vortex.

Acknowledgements

The authors would like to acknowledge the support of the National Science Foundation of China (No. 51406003) and the National Science and Technology Major Project (J2019-II-0019-040).

References

[1] Denton J.D., Loss mechanisms in turbomachines. Journal of Turbomachinery, 1993, 115(4): 621–656.

[2] Yang H.K., Zhang W.H., Zou Z.P., et al., The development and applications of a loading distribution based tip leakage loss model for unshrouded gas turbines. Journal of Turbomachinery, 2020, 142(7): 1–29.

[3] Yang H.K., Zhang W.H., Zou Z.P., Effects of loading distribution on turbine tip leakage losses. Journal of Engineering Thermophysics, 2020, 41(01): 113–121. (in Chinese)

[4] Dey D., Camci C., Aerodynamic tip desensitization of an axial turbine rotor using tip platform extensions. ASME Turbo Expo 2001: power for land, sea, and air, New Orleans, United States of America, 2001, V001T03A069.

[5] Zhou C., Hodson H., Tibbott I., et al., Effects of winglet geometry on the aerodynamic performance of tip leakage flow in a turbine cascade. Journal of Turbomachinery, 2013, 135(5): 051009.

[6] Coull J.D., Atkins N.R., Hodson H.P., Winglets for improved aerothermal performance of high pressure turbines. Journal of Turbomachinery, 2014, 136(9): 091007.

[7] Bunker R.S., Axial turbine blade tips: function, design, and durability. Journal of Propulsion and Power, 2006, 22(2): 271–285.

[8] Key N.L., Arts T., Comparison of turbine tip leakage flow for flat tip and squealer tip geometries at high-speed conditions. Journal of Turbomachinery, 2006, 128(2): 213–220.

[9] Jun L.I., Sun H., Wang J., et al., Numerical investigations on the steady and unsteady leakage flow and heat transfer characteristics of rotor blade squealer tip. Journal of Thermal Science, 2011, 20(4): 304–311.

[10] Liu J.J., Li P., Zhang C., et al., Flowfield and heat transfer past an unshrouded gas turbine blade tip with different shapes. Journal of Thermal Science, 2013, 22(2): 128–134.

[11] Li W., Jiang H., Zhang Q., et al., Squealer tip leakage flow characteristics in transonic condition. Journal of Engineering for Gas Turbines and Power, 2014, 136(4): V06AT36A029.

[12] Ma H.W., Wang L.X., Experimental study of effects of tip geometry on the flow field in a turbine cascade passage. Journal of Thermal Science, 2015, 1(1): 1–9.

[13] Dey D., Kavurmacioglu L., Camci C., Tip desensitization of an axial turbine rotor using partial squealer rims. Turbine blade tip design and tip clearance treatment. VKI Lecture Series, 2004, 2: 19–23.

[14] Acharya S., Yang H., Prakash C., et al., Numerical study of flow and heat transfer on a blade tip with different leakage reduction strategies. ASME Turbo Expo 2003, collocated with the 2003 International Joint Power Generation Conference, Atlanta, United States of America, 2003, Paper No. GT2003-38617, pp. 471–480.

[15] Krishnababu S.K., Newton P.J., Dawes W.N., et al., Aerothermal investigations of tip leakage flow in axial flow turbines—Part I: effect of tip geometry and tip clearance gap. Journal of Turbomachinery, 2009, 131(1): 011006.

[16] Zhou C., The tip leakage flow of an unshrouded high pressure turbine blade with tip cooling. Journal of Turbomachinery, 2011, 133(4): 929–942.

[17] Yang D.L., Feng Z.P., Tip leakage flow and heat transfer predictions for turbine blades. ASME Turbo Expo 2007: Power for Land, Sea, and Air, Montreal, Canada, 2007, Paper No. GT2007-27728, pp. 589–596.

[18] Yang D., Yu X., Feng Z., Investigation of leakage flow and heat transfer in a gas turbine blade tip with emphasis on the effect of rotation. Journal of Turbomachinery, 2010, 132(4): 041010.

[19] Virdi A.S., Zhang Q., He L., et al., Aerothermal performance of shroudless turbine blade tips with relative casing movement effects. Journal of Propulsion and Power, 2015, 31(2): 527–536.

[20] Mischo B., Behr T., Abhari R.S., Flow physics and profiling of recessed blade tips: impact on performance and heat load. Journal of Turbomachinery, 2008, 130(2): 021008.

[21] Zhou C., Effects of endwall motion on thermal performance of cavity tips with different squealer width and height. International Journal of Heat and Mass Transfer, 2015, 91: 1248–1258.

[22] Zou Z., Shao F., Li Y., et al., Dominant flow structure in the squealer tip gap and its impact on turbine aerodynamic performance. Energy, 2017, 138: 167–184.

[23] Paty M., Lavagnoli S., A novel vortex identification technique applied to the 3D flow field of a high-pressure turbine. Journal of Turbomachinery, 2020, 142(3): 031004.

[24] Gao J., Zheng Q., Effect of squealer tip geometry on rotor blade aerodynamic performance. Acta Aeronautica et Astronautica Sinica, 2013, 34(2): 218–226.

[25] Lomakin N., Granovskiy A., Belkanov V., et al., Effect of common blade tip squealer designs in terms of tip clearance loss control. ASME 2013 Turbine Blade Tip Symposium, Hamburg, Germany, 2014, V001T03A005.

[26] Lomakin N., Granovskiy A., Shchaulov V., et al., Effect of various tip clearance squealer design on turbine stage efficiency. ASME Turbo Expo 2015: Turbine Technical Conference and Exposition, Montreal, Canada, 2015, V02AT38A017.

[27] Zhou C., Hodson H., Squealer geometry effects on aerothermal performance of tip-leakage flow of cavity tips. Journal of Propulsion and Power, 2012, 28(3): 556–567.

[28] Senel C.B., Maral H., Kavurmacioglu L.A., et al., An aerothermal study of the influence of squealer width and height near a HP turbine blade. International Journal of Heat and Mass Transfer, 2018, 120: 18–32.

[29] Prakash C., Lee C.P., Cherry D.G., et al., Analysis of some improved blade tip concepts. Journal of Turbomachinery, 2006, 128(4): 639–642.

[30] De Maesschalck C., Lavagnoli S., Paniagua G., et al., Heterogeneous optimization strategies for carved and squealer-like turbine blade tips. Journal of Turbomachinery, 2016, 138(12): 121011.

[31] Cernat B.C., Pátý M., De Maesschalck C., et al., Experimental and numerical investigation of optimized blade tip shapes—Part I: Turbine rainbow rotor testing and numerical methods. Journal of Turbomachinery, 2019, 141(1): 011006.

[32] Pátý M., Cernat B.C., De Maesschalck C., et al., Experimental and numerical investigation of optimized blade tip shapes—Part II: tip flow analysis and loss mechanisms. Journal of Turbomachinery, 2019, 141(1): 011007.

[33] Qi L., Zou Z., Liu H., et al., Upstream wake-secondary flow interactions in the endwall region of high-loaded turbines. Computers & Fluids, 2010, 39(9): 1575–1584.

[34] Wang Y., Zhang W., Cao X., et al., The applicability of vortex identification methods for complex vortex structures in axial turbine rotor passages. Journal of Hydrodynamics, 2019, 31(4): 700–707.

[35] Liu C.Q., Wang Y.Q., Yang Y., et al., New omega vortex identification method. Science China Physics, Mechanics and Astronomy, 2016, 59(8): 684711.

[36] Zhang Q., Du J., Li Z., et al., Entropy generation analysis in a mixed-flow compressor with casing treatment. Journal of Thermal Science, 2019, 28(5): 915–928.